Temperature and Textures of Ash Flow Surfaces:
Shiveluch, Kamchatka, Russia
4 June 2004

Michael Ramsey
University of Pittsburgh
Department of Geology and Planetary Science
SRCC 200
Pittsburgh, PA 15260
mramsey@pitt.edu

Key Words: Shiveluch, Thermal Infrared, Pyroclastic Flows, Lava Domes, ASTER

Activity Description

Shiveluch is the northernmost active volcano in the Kurile-Kamchatka arc. It is also the most active and one of the largest in Kamchatka, erupting several times per year on average (Fedotov and Masurenkov, 1991). Activity can range from andesite dome growth/collapse, to ash plume producing Vulcanian explosions, to sub-Plinian explosive eruptions. The summit caldera is breached to the south, which funnels most block and ash flows in that direction. Larger-scale dome collapse events can occur infrequently (the last in 1964) producing debris avalanche deposits that have created the large unvegetated plain south of the caldera (Fig. 1).

During 2004, Shiveluch was in a continual state of unrest including above-background seismicity, lava-dome growth with associated pyroclastic flows (PF), and frequent ash plumes that extended hundreds of kilometers. During the early part of the year, numerous thermal anomalies were detected with both low spatial, high temporal resolution instruments such as AVHRR and MODIS as well as high spatial, lower temporal resolution instruments such ASTER and Landsat ETM+ (BGVN, 2004). Activity increased in May and during the early morning hours of 10 May, a series of strong ash explosions occurred at the summit. Seismic activity, video and visual observations confirmed the explosive eruption, which sent ash to 8-11 km altitude and a plume over 450 km to the southeast. Pyroclastic flows and lahars were observed extending ~9 km downslope. This activity continued for several days (Fig. 2), and a field-based reconnaissance was conducted on 21 May by the Russian Institute of Volcanology and Seismology (IVS). The emplacement mechanisms, temperatures, block sizes and numerous photographs were all recorded (Girina et al., 2004). The team noted smaller pyroclastic flows consisting of finer-grained juvenile material as well as coarser-grained block and ash flows (Fig. 3). The block and ash flow deposits were visibly-darker and concentrated in the central part of the larger PF deposit. The run-out distance of these deposits was ~ 10 km and the total volume was estimated to be ~ 0.05 km^3.

Data Processing Description

The ASTER thermal infrared (TIR) instrument is unique among orbital sensors in its spatial, spectral and radiometric resolution. The TIR data are collected at 90m/pixel in five spectral bands and in 12-bit quantization. That resolution limits the number of saturated pixels, which only occur where pixel integrated brightness temperatures exceed 100 °C. ASTER acquired nighttime images on 11 May and 20 May at approximately 23:00 local time and daytime images on 21 May and 4 June at approximately 11:30 local time. The 4 June daytime

scene used for this study was acquired at 11:37:59 local time and available for analysis ~5 hours later. The ENVI © software package was used to atmospherically-correct the TIR data for attenuation and emitted downwelling radiance. The surface radiance was then separated into emissivity and pixel-integrated brightness temperature, which were both analyzed. The temperature in the scene ranged from -8 °C on the highest slopes to several saturated pixels at the dome. The large ash flow deposit was approximately 10 °C above the temperature of the surrounding plains and therefore easily visible in the temperature image (Fig. 4). The emissivity data can be used for both compositional and textural mapping using approaches described in Ramsey and Christensen (1998) and Ramsey and Fink (1999). The primary spectral absorption band (emissivity low) in silicate minerals is produced by the Si-O bond and falls within the 8-12 μm region. Changes in the position or morphology of this band can indicate compositional variability and changes in the depth is related more to the micron scale roughness (MSR) of the surface. The ASTER emissivity data were deconvolved or unmixed using the spectra of a volcanic glass and a spectrally-featureless blackbody as end-members. The percentage of blackbody serves as a proxy for the degree of MSR or surface vesicularity. These values were contoured in 5% increments from 30 – 45% and overlain on the ASTER VNIR color image (Fig. 5).

Interpretation

The hottest temperatures correspond to four saturated TIR pixels located on the summit dome. In order to raise the pixel integrated brightness temperature above the saturation limit, a significant fraction of the pixel must contain very hot material (e.g., active dome extrusion). Estimates based on field-based photography from 21 – 29 May period indicated new dome growth was occurring at a rate of 4-5 m/day (Girina et al., 2004). Using the spatial distribution of the saturated TIR pixels and accounting for the average slope of the dome, the linear extrusion rate was also calculated from the ASTER temperature data. The length of hot material emplaced over the 26 days from eruption to the ASTER acquisition was 214 ± 17 m, which corresponds to a rate between 7.6 – 8.9 m/day.

Derived from the ASTER emissivity data, the modeled MSR of the deposit furthest from the dome shows a concentric pattern of lower values (~ 15%) toward the center (i.e., blockier, less vesicular material). This deposit also retained its heat longer than the deposit to the north indicating a higher thermal inertia. This pattern of MSR is also consistent with the field evidence that showed the deposit had a lower albedo, contained more blocks, and had an overall coarser size fraction than the surrounding PF deposits. The lower MSR values are also similar to those extracted over the new dome, which indicates a potential match between the dome lava and the blocks in the deposit. The PF deposit closer to the dome had a higher MSR value on average (40-45%), is therefore more likely ash-rich, and was produced by eruptions following the dome collapse.

Near Real-Time Analysis

The numerous thermal anomalies detected by AVHRR following the May eruption triggered the ASTER Urgent Request Protocol (UPR), which increased the number of ASTER observations by more than 50%. The use of near real-time thermal anomaly detections to trigger more detailed observations has been in place since 2004 and has proven especially effective for the eruptions in Kamchatka (Duda et al., 2009). Of the six ASTER observations (two day/four night) attempted in the month following the 10 May eruption, the summit of Shiveluch was only

obscurred by significant cloud cover on two of those dates. The first clear ASTER acquisition took place at night only 33 hours after the eruption 11 May 2004. For this study, the clearest daytime observation (4 June 2004) was used.

In Depth Analysis

The high spatial resolution of the ASTER VNIR and TIR data coupled with the relatively quick response time from the URP program provides detailed information of recent eruptions in the North Pacific. A simple analysis of the temperature data revealed the smaller-scale thermal patterns of the new lava dome and recently-emplaced flows and lead to an estimate of the dome's extrusion rate and thermal response of the flow deposits.

The ability to acquire multispectral emissivity data makes the ASTER TIR instrument even more significant. The emissivity was modeled using a two end-member deconvolution approach to estimate the surface texture or micron-scale roughness. The MSR values confirmed the field evidence of the deposit types and their emplacement mechanisms. The concentric pattern of a lower MSR core surrounded by finer grain, higher MSR material found in the southern-most flow deposit could be interpreted one of two ways. The deposit could have been formed as one event with the blocks being concentrated in the center of the ash-rich material. Alternatively, there could have been two emplacement events – an ash-rich PF surge deposit followed by the collapse of the dome and emplacement of the block and ash flow over the PF deposit. The deposit at the higher elevation was not analyzed in the field but appears to be mostly ash-rich; indicating there could have been multiple events of ash and block rich deposits emplaced over the course of the May 2004 eruption.

Associated Publications

Bulletin Global Volcanism Network (BGVN), February 2005. Shiveluch Volcano, Smithson. Inst., 30:02.

Bulletin Global Volcanism Network (BGVN), June 2005. Shiveluch Volcano, Smithson. Inst., 30:06.

Fedotov, S.A., Masurenkov, Y.P., 1991. Active Volcanoes of Kamchatka, vol. 1. Nauka, Moscow, p. 713.

Girina, O.A., Senyukov, S.L., Demyunchuk, Y.V., Khubunaya, S.A. and Ushakov, S.A., 2004. The eruption of Sheveluch Volcano, Kamchatka, on May 09, 2004, in Proc. of the 4th Biennial Workshop on Subduction Processes in the Japan-Kurile-Kamchatka-Aleutian Arcs, p. 17.

Ramsey, M.S. and Fink, J.H., 1999. Estimating silicic lava vesicularity with thermal remote sensing: A new technique for volcanic mapping and monitoring, Bull. Volc. 61, 32-39.

Ramsey, M.S. and Christensen, P.R., 1998. Mineral abundance determination: Quantitative deconvolution of thermal emission spectra, J. Geophys. Res., 103, 577-596.

Figures

Fig. 1. Helicopter-based photograph taken on 21 August 2005 of Shiveluch Volcano looking to the northeast. The older Stary Shiveluch is seen in the background with moderate snow cover and the younger active dome complex of Molodoy Shiveluch is in the foreground. Numerous debris avalanche deposits, pyroclastic flows and block and ash flows make up the unvegetated plain to the south of the breached horseshoe-shaped summit caldera.

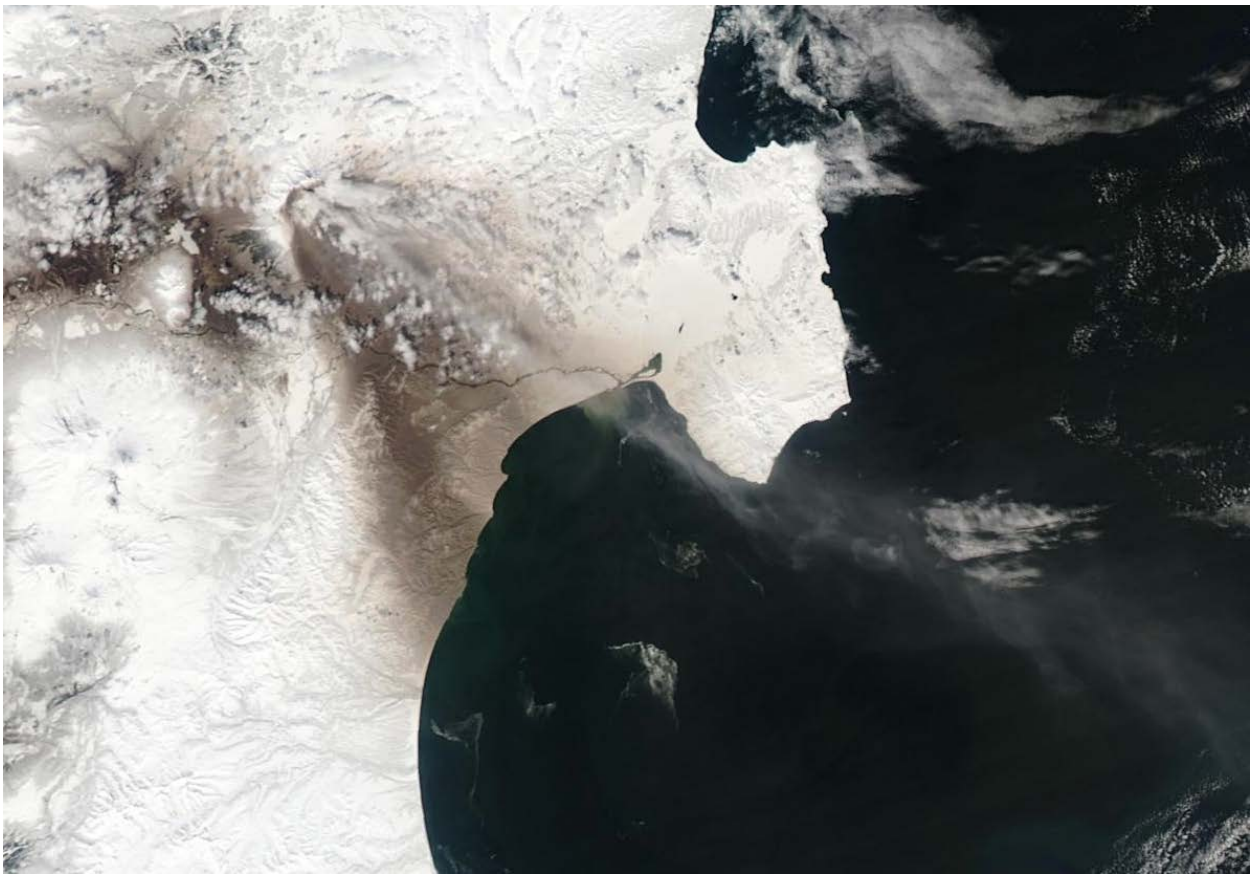

Fig. 2. Visible color image acquired on 11 May 2004 by the Moderate Resolution Imaging Spectroradiometer (MODIS) on the NASA Aqua satellite. The active ash plume drifting to the southeast over the Pacific Ocean can be seen in addition to the ash-covered snow deposited following the eruption of 10 May 2004.

Fig. 3. Field-based photographs of the new deposits taken on 21 May 2004 by Sergey Ushakov and Olga Girina during the first reconnaissance following the 9 May 2004 eruption. **(A)** View from the southern flank of the volcano looking to the south and showing the small pyroclastic flows (lighter tones) and the larger block and ash flows (darker tones). **(B)** View of the pyroclastic flow deposit looking toward the summit. The flow was made up of juvenile material and few blocks. **(C)** View of the block and ash flow deposit looking toward the summit. This deposit consisted of numerous dense blocks of older dome material.

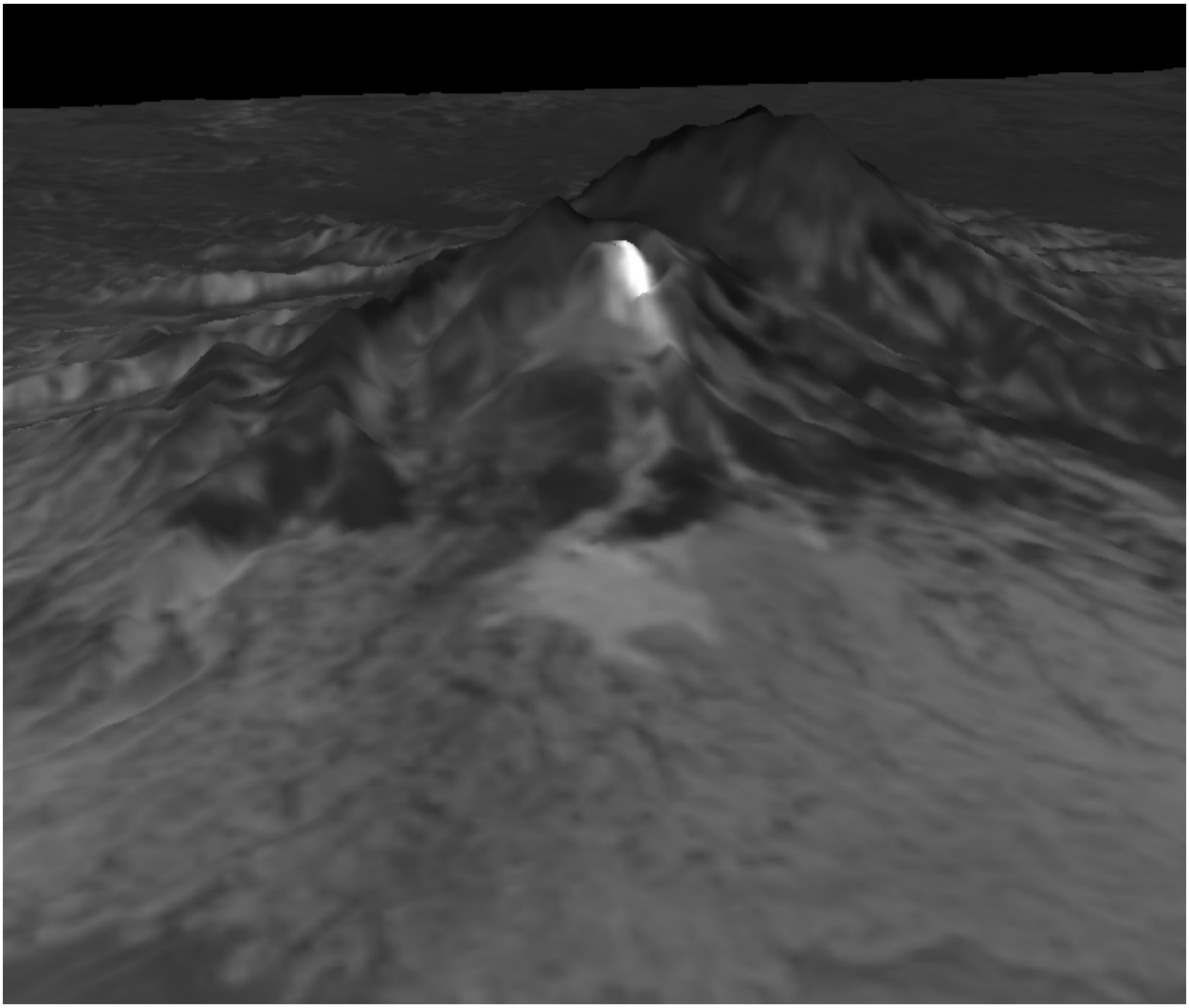

Fig. 4. ASTER thermal infrared pixel-integrated brightness temperature image (90 m/pixel spatial resolution) acquired on 4 June 2004 and draped over an ASTER-derived DEM from the same date. The new dome and block and ash flow deposit in the foreground are both visible. Nearly one month after emplacement, the deposit is still thermally-elevated (T_{avg} = 25 °C) above the temperature of the surrounding plains (T_{avg} = 15 °C). The new dome, indicated by the highest temperatures, has an average extrusion rate of 8.3 m/day.

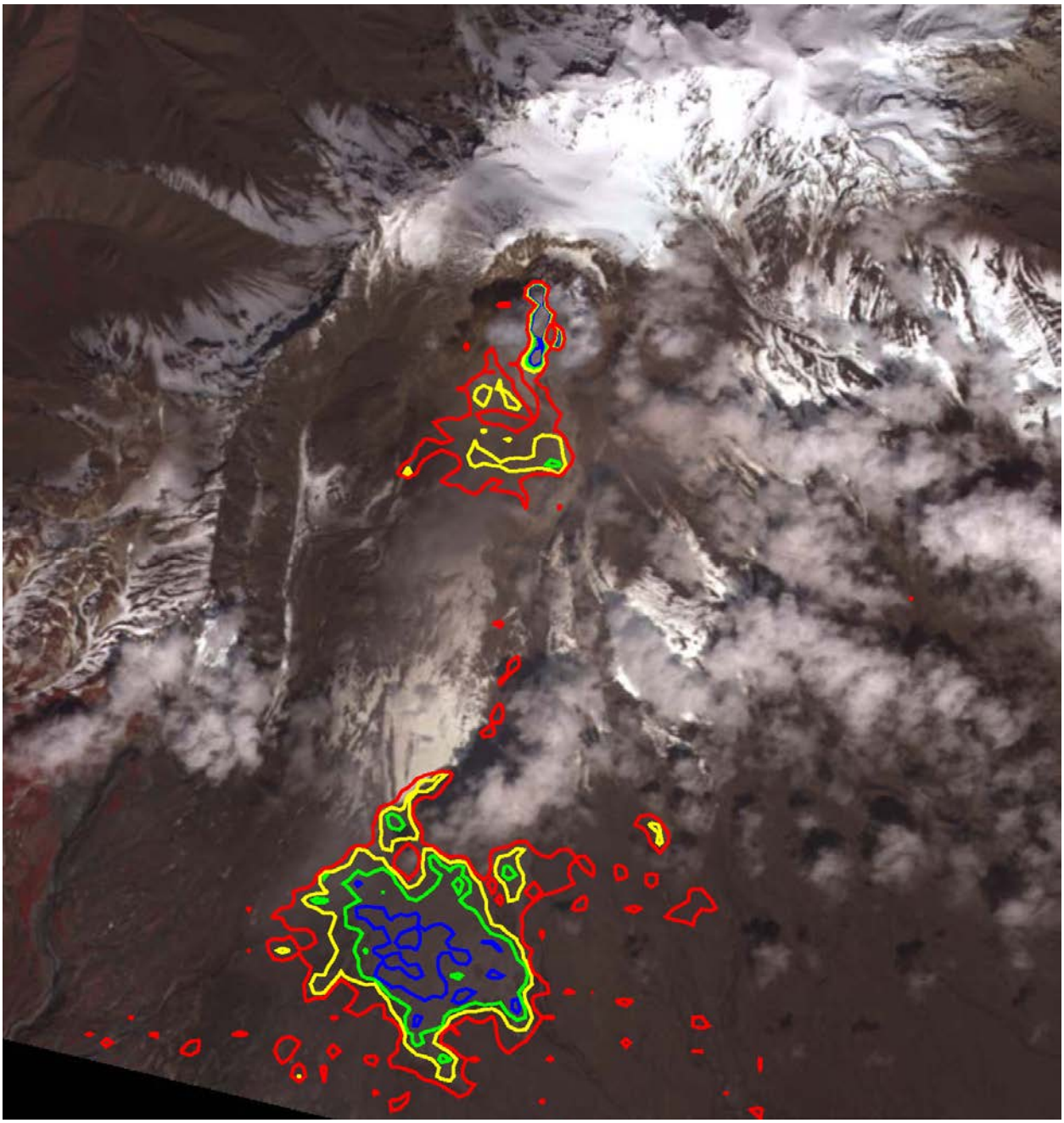

Fig. 5. Micron-scale roughness (MSR) values of the new flow deposits modeled from the ASTER TIR emissivity data. MSR values, a proxy for surface vesicularity, are contoured in 5% increments (30% = blue; 35% = green; 40% yellow; and 45% = red) and draped over the 15 meter ASTER VNIR image. The deposit to the south shows a concentric pattern of lower MSR in the center that reflects the denser block and ash deposit; whereas the northern deposit has higher MSR values indicative of a juvenile pyroclastic flow deposit. Portions of the new dome also have lower MSR values similar to those found in the larger flow deposit.